Underlying Adsoprtion Mechanisms of Water in Hydrophobic and Hydrophilic Zeolite Imidazolate Frameworks: ZIF-71 and ZIF-90

ARTICLE *in* THE JOURNAL OF PHYSICAL CHEMISTRY C · SEPTEMBER 2015

Impact Factor: 4.77 · DOI: 10.1021/acs.jpcc.5b07360

2 AUTHORS:

Sofia Calero

Universidad Pablo de Olavide

164 PUBLICATIONS **3,063** CITATIONS

SEE PROFILE

Paula Gómez-Álvarez

Universidad Pablo de Olavide

26 PUBLICATIONS **38** CITATIONS

SEE PROFILE

Underlying Adsorption Mechanisms of Water in Hydrophobic and Hydrophilic Zeolite Imidazolate Frameworks: ZIF-71 and ZIF-90

S. Calero and P. Gómez-Álvarez*

Department of Physical, Chemical and Natural Systems. Universidad Pablo de Olavide.

ES-41013 Seville, Spain

*E-mail: pgomalv1@upo.es

Abstract

The hydration of porous materials is relevant for separation, transport and catalysis purposes, among others. In this respect, Zeolitic Imidazolate Frameworks (ZIFs) have received considerable attention since they have shown remarkably resistance to water, as well as to other organic solvents. Studies on water adsorption in ZIFs are however relatively scarce and primarily focused on the effect of the host composition and porosity on their hydrophobic or hydrophilic nature. In this work, we explore the underlying adsorption mechanisms of water in ZIF-71 and ZIF-90, which are experimentally known structures. These ZIFs have been reported hydrophobic and hydrophilic, respectively. We conducted Monte Carlo simulations using previously validated models and force fields to compute the adsorption isotherms of water in both ZIFs at room temperature. Although the polar functional group in ZIF-90 leads to adsorption in the gas phase, a following rapid cage filling occurs as in ZIF-71. A consistent description of this phenomenon is provided in terms of hydrogen bonding formation between water molecules. In the low coverage-regime, the preferential adsorption sites are identified and interactions with water comprehensively characterized.

Keywords: cage filling, hydrogen bonds, MOFs, Monte Carlo simulations, adsorption energy.

1. Introduction

In the last decade, there has been an exponential growth of interest in Metal Organic Frameworks (MOFs) because of the versatility in tuning their structures and functionalities.[1] MOFs can be synthesized from various inorganic clusters and organic linkers, thus possess a wide range of surface area and pore size[1] Consequently, MOFs have been considered as potential materials for storage, separation, catalysis, and other emerging applications.[2-7] Most experimental and theoretical studies for the uses of MOFs have been focused on gas storage and separation,[8-11] and only very few studies[12-14] were conducted using MOFs for adsorption of water despite being of great importance in a variety of chemical and industrial processes. For applications in aqueous media, chemically stable MOFs are desired. However, most common MOFs cannot meet this requirement. Recently, the Zeolitic Imidazolate Frameworks (ZIFs) have attracted considerable attention since they are known to generally exhibit permanent porosity and display a high chemical and also thermal stability.[15,16] ZIFs are a subset of MOFs with three-dimensional structures connected in a tetrahedral arrangement by metal centers, such as Zn or Co, and organic bare or functionalized imidazolate linkers.[17,18] They have topologies resembling inorganic zeo-type networks and exhibit similar structural properties. Intriguingly, the substitution of oxygen atoms in zeolites with tunable organic linkers leads to extra-large cavities. The molecular design of ZIFs is currently very active, and exploring their scope for practical applications is still in a newborn stage. While much attention has been paid to the adsorption of small gases and hydrocarbons,[17-24] works on water adsorption as well as other organic solvents using ZIFs are still very limited. Among the experimental works, Küsgens *et al*.[25] reported the water vapor adsorption isotherm at room temperature for ZIF-8 demonstrating the strong hydrophobic character of this material and its remarkable

hydrothermal stability. Guillaume Ortiz *et al*.[26] investigated the energetic performance of ZIF-71 in comparison with ZIF-8 in high pressure liquid water intrusion–extrusion experiments. Zhang *et al*.[27] studied the impact of ZIF-8 hydrophobicity for the separation of ethanol from water, predicting a good adsorption selectivity. Lively *et al*.[28] presented the isotherm of water adsorption on ZIF-71 and corroborated the hydrophobicity of this material, with very low water uptake at pressures below the bulk saturation pressure. On the theoretical side, with the tremendous growth of computational power, molecular simulation has increasingly become a robust tool to assist experiments. Nalaparaju *et al*.[29] conducted a computational study of water adsorption in hydrophobic ZIF-71, as well as in hydrophilic Na-rho-ZMOF (a MOF with anionic framework and Na^+ extra-framework cations). Amrouche *et al*.[30] studied the low-pressure adsorption of water in a series of ZIFs by using the ideal heat of adsorption and Henry constant as descriptors of hydrophobicity or hydrophilicity. Zhang *et al*.[31] published a study of water and also alcohol adsorption in ZIF-8, ZIF-71 and ZIF-90 approached to bio-alcohol recovery. They found the hydrophobic ZIF-8 and ZIF-71, especially the latter, more suitable to this end. Ortiz *et al*.[32] demonstrate, by means of Grand Canonical Monte Carlo simulations on different members of the ZIF family, how topology, geometry, and linker functionalization drastically affect the water adsorption properties of these materials, tweaking the ZIFs from hydrophobic to hydrophilic. Zhang *et al*.[33] recently performed a molecular simulation study of separation of ethanol from water in ZIF-8,-25, -71, -90, -96 and -97, revealing the importance of the functional groups for the efficacy of such separation.

In the previous works, the hydrophobic and hydrophilic nature of a number of ZIF materials has been determined, and also rationalized in terms of topology, geometry, and linker functionalization. A clear fundamental understanding of the microscopic properties

of water molecules within these porous solids connecting with the observed macroscopic behavior is likewise indispensable, and comprehensively addressed in this work. We used molecular simulation techniques[34] to study the adsorption performance, and the underlying physics, of water in ZIF-71 and ZIF-90, which are well-known for their hydrophobic and hydrophilic characters, respectively. The adsorption isotherms of water in both ZIFs were computed using Monte Carlo simulations in the Grand Canonical ensemble at room temperature. Water-water and water-ZIF interactions characterizing the adsorption mechanisms were quantitatively evaluated from energetic factors, and structural properties such as the Radial Distribution Functions (RDFs) or Hydrogen-Bonded (HB) statistics. The latter have been calculated in the basis of a specific criterion of hydrogen bonding formation applied along the simulation.

2. Methods

2.1. Structures

ZIF-71 [$Zn(dcIm)_2$, where dcIm = 4,5-dichloroimidazolate] possesses a RHO-type topology consisting on a three-dimensional pore network formed by large α cages of 16.8 Å interconnected via small windows of 4.8 Å in a cubic body-centered arrangement.[18] The cell lengths of ZIF-71 are: a = b= c =28.554 Å, and angles α = β = γ = 90º. ZIF-90 [$Zn(icaIm)_2$, where icaIm = imidazole-2-carboxyaldehyde] belongs to SOD topology with an extended 3-D structure with a pore window opening of 3.5 Å and a pore size of 11.2 Å[35] The material is made of uniform micropores containing unsaturated –CHO aldehyde functional groups. The cell parameters of ZIF-90 are: a = b= c= 17.272 Å, and α = β = γ = 90º. Figure 1 illustrates the atomic structures of both ZIFs.

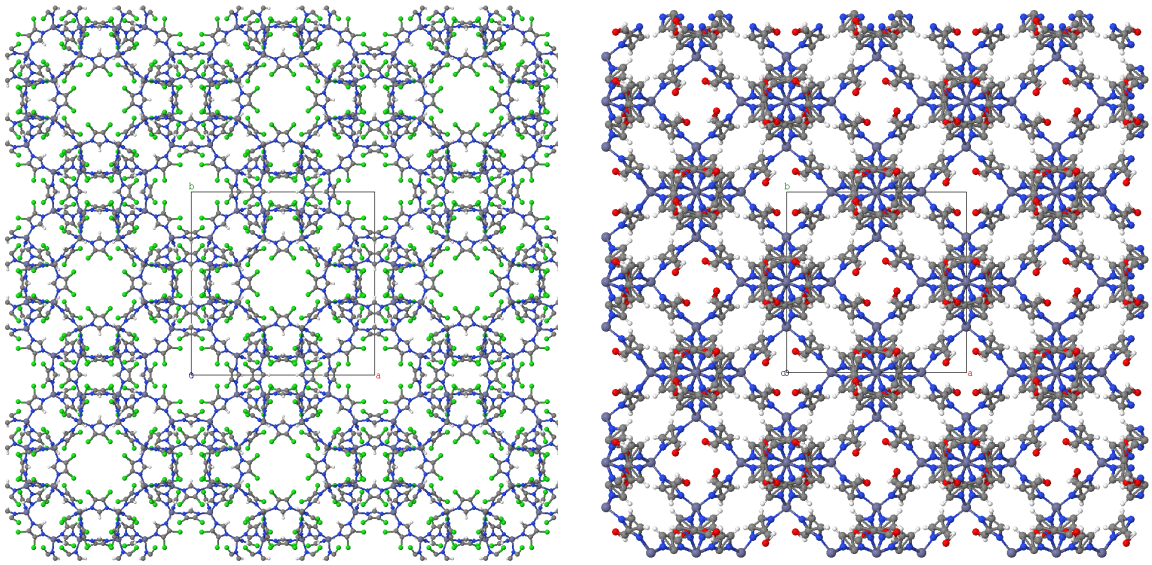

Figure 1. Atomic structures of ZIF-71 (left) and ZIF-90 (right). Cl: green, C: grey, H: white, O: red, N: blue, Zn: cyan. The size is not in the same scale.

Table 1 collects a number of structural properties characterizing the pore sizes and the accessible space (for a probe radius of 1.7 Å) of the targeted ZIFs. Particularly, we report the Pore Limiting Diameter (PLD), the Largest Cavity Diameter (LCD), the Accessible Volume (AV), and the Accessible Surface Area (ASA). They were computed using Zeo++,[36] a code for a geometric analysis of crystalline porous materials. The PLD and LCD agree quite well with the experimental values commented above. The accessible volume is also consistent with that reported in previous works.[33] Note that although the LCD of ZIF-71 is larger than this for ZIF-90, the free volume and surface area are lower. To give an idea on how the available space distribute within the pores, Figure S1 of the Electronic Supporting Information (ESI) displays the Pore Size Distributions of both ZIFs.

Table 1. Geometric properties of the studied ZIFs computed using Zeo++ code.[36] Accessible Volume and Surface Area are computed for a probe radius of 1.7 Å.

	Density / kg·m^{-3}	**PLD / Å**	**LCD / Å**	**AV / cm^3·g^{-1}**	**ASA / m^2·g^{-1}**
ZIF-71	1155	5.4	17.0	0.1725	1120
ZIF-90	988	3.5	11.4	0.1916	1526

2.2. Models and force fields

Guest water molecules were described by the rigid, non-polarizable, and five-site TIP5P/Ew model.[37] The host structures were treated as rigid frameworks since the importance of flexibility on adsorption properties has only a marginal effect. ZIF–water interactions were described by a classical force field including the repulsion-dispersion energy, modeled by Lennard-Jones 6-12 potentials, and Coulombic interactions, modeled by point charges on the framework atoms of the ZIFs. Both the Lennard-Jones parameters and the atomic point charges of the ZIFs were taken from the earlier work of Zhang *et al.*,[33] who considered the DREIDING force field[38] for the L-J parameters and calculated atomic charges using the Density Functional Theory (DFT). Lorentz-Berthelot mixing rules[34] were used to obtain the parameters characterizing L-J cross interactions.

2.3. Monte Carlo simulations

Monte Carlo simulations of water at 298 K were performed using RASPA code[39,40] and the above-described models and force fields. The adsorption of water in the ZIFs was

computed using the grand canonical ensemble (μVT), in which temperature, volume and chemical potential are kept fixed. The latter is related to the imposed fugacity, from which pressure can be determined using the Peng-Robison equation of state.[41] The number of unit cells for each structure was chosen in order to get a simulation box larger than twice the Lennard-Jones cut-off radius, which was set to 12 Å: The simulation box thus contained one unit cell of ZIF- 71, and eight unit cells (2×2×2) for ZIF-90. The periodic boundary conditions[34] were exerted in three dimensions, and long-range electrostatic interactions were evaluated using the Ewald summation technique.[34] Three types of trial moves were randomly attempted, namely molecular displacement (25%), rotation (25%), and a swap between reservoirs (50%) including creation and deletion with equal probability. Each point of the isotherms was obtained after equilibration runs of 50 000 cycles followed by production runs of 500 000 cycles. Additional simulations in the NVT ensemble were carried out to obtain results for specific low numbers of molecules.

2.4. Criterion of hydrogen-bonding formation

For an accurate estimation of the HB network of water, we applied a geometric criterion[42] of HB definition over a considerable number of the computed-generated configurations along the simulation. According to which, a hydrogen bond between two water molecules exists when the r_{OO} and r_{OH} intermolecular separations are lower than certain threshold values, which are given by the average distances of the first minimum location in the respective g_{OO} and g_{OH} functions (3.6 Å and 2.4 Å),[43] and limitation to the angle (30 º) between intermolecular O···O and covalent O-H vectors is fulfilled.

3. Results and discussion

Figure 2 shows the adsorption isotherms of water in ZIF-71 and ZIF-90. The used models and force fields allow to reproduce quite accurately the experimental behavior,[31] as previously shown in Zhang *et al.*[33] On the one hand, the isotherms of water in ZIF-71 belong to *S*-shaped type V, which signifies the adsorption of the weakly interacting adsorbate in a microporous structure. Water has vanishingly small adsorption at low pressures, and a sharp increase in adsorption approaching saturation rapidly is observed above the saturation pressure p_0 (adsorption in the liquid phase). In particular, this condensation transition occurs at about 25 kPa ($p/p_0 \approx 8$). The described behavior is typical of hydrophobic materials. On the other hand, water uptake is initially negligible in ZIF-90 but sharply increases beyond 1 kPa (adsorption in the gas phase), which suggests its hydrophilic nature. More specifically, as it is clearly apparent from the inset figure, water adsorption occurs from p/p_0 of about 0.4, which is slightly larger than the experimental value[31] (p/p_0 of about 0.3). At relative pressure of 1, the water loading in ZIF-90 is well coincident with experiments[31] (20 mol·kg^{-1}, approximately). At saturation, it notably overcomes that in ZIF-71 at saturation. This is likely induced by the larger porosity of ZIF-90 (Table 1) as well as to stronger water-ZIF interactions induced by the –CHO groups. On the basis of the lower onset pressure of water adsorption in ZIF-90 and the larger adsorption capacity, we can state that this ZIF represents a better option for applications of water adsorption and storage. Although the deviations in ZIF-90 and ZIF-71 are relatively large, they exhibit a common feature of adsorption: Cage-filling occurs with a sharp increase in the uptake. To illustrate this, we plot in Figure 3 the density contours (XY plane) of water in the simulation box of ZIF-71 (top) and ZIF-90 (bottom) for two low

(onset adsorption) close values of fugacity. The rapid uptake mechanism in both ZIFs is evident from the pictures. In this sense, ZIF-90 shows an amphiphilic character, with some parts of its internal surface hydrophilic (adsorption in the gas phase), and some parts hydrophobic (abrupt condensation transition).

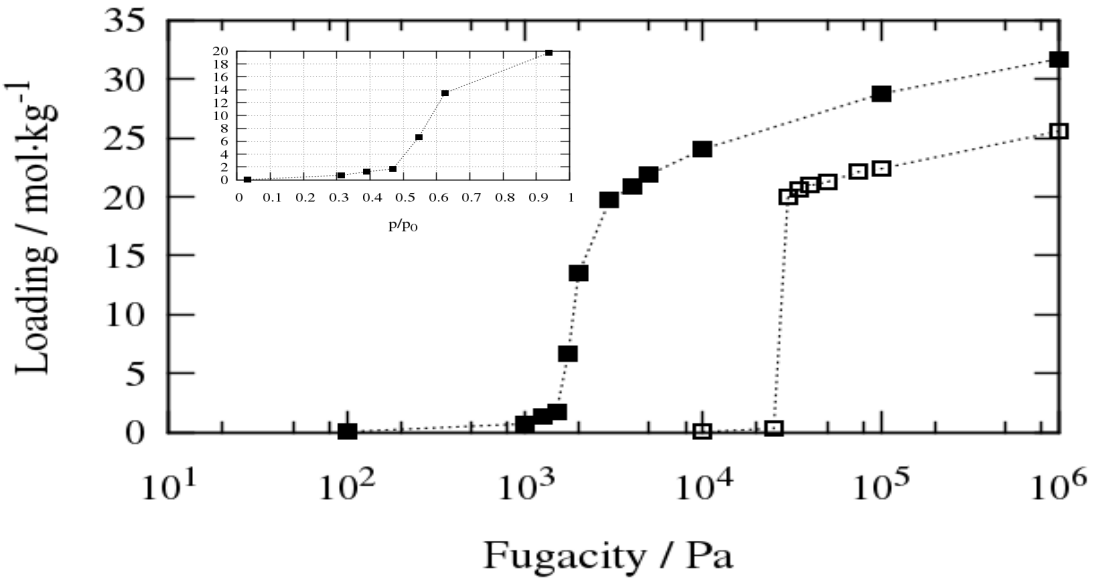

Figure 2. Adsorption isotherms of water in ZIF-71 (empty squares) and in ZIF-90 (full squares). Inset figure shows the vapor adsorption isotherm for ZIF-90 ($p_0 = 3.2$ kPa).

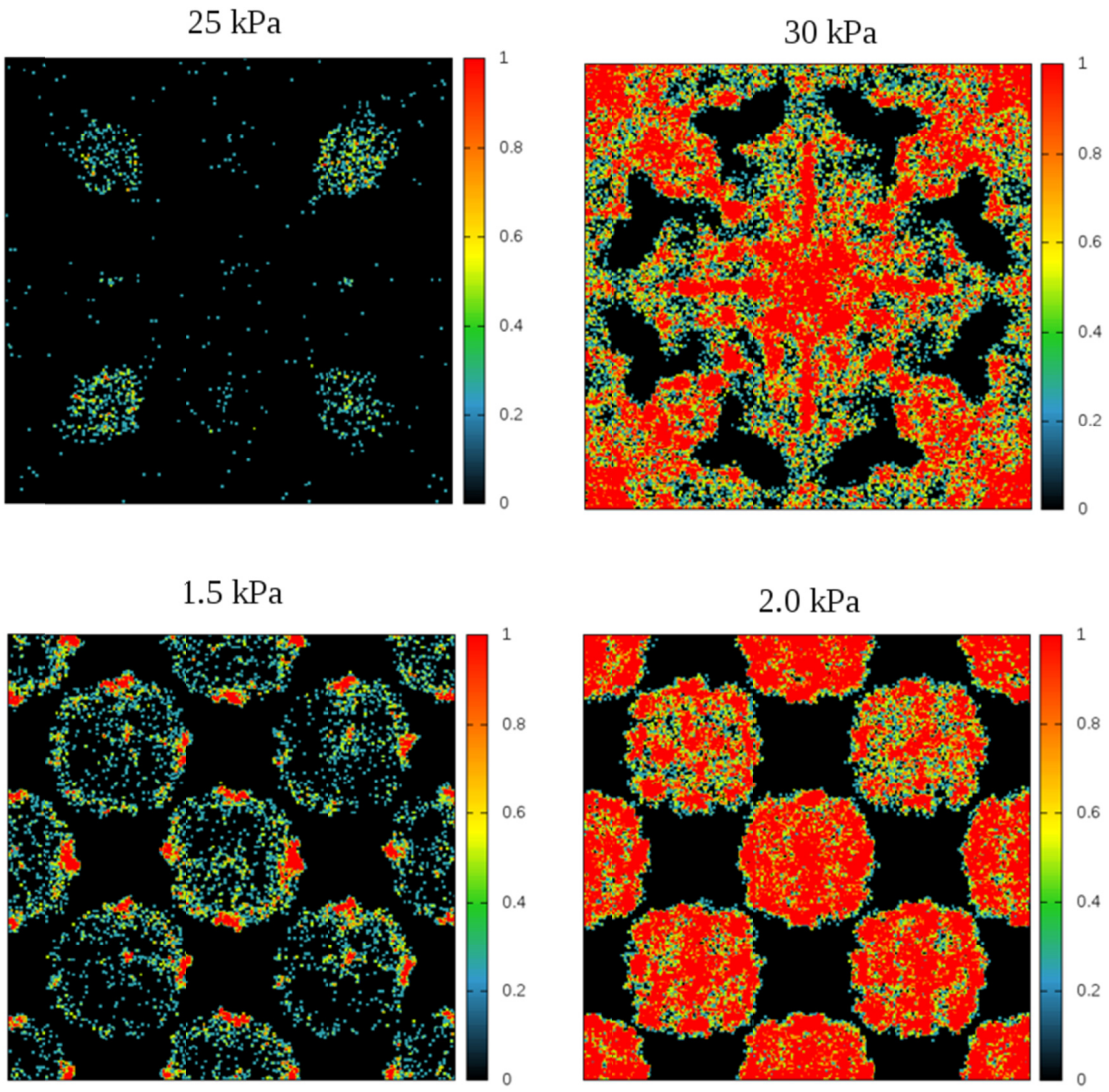

Figure 3. Density contours (XY plane) of water molecules in ZIF-71 (top) at 25 kPa and 30 kPa, and ZIF-90 (bottom) at 1.5 kPa and 2.0 kPa.

To deeply elucidate the described water adsorption performance of both ZIFs, we comprehensively analyzed the systems at the molecular scale in terms of a series of energetic and structural properties. In Figures 4 and 5, we quantitatively evaluate the energetic factors during the adsorption process. Figure 4 reports the average adsorption

energy as a function of the loading. Inset figure shows this magnitude for a low number of molecules from NVT calculations to examine the very low coverage regime. The values for a single water molecule represent the heats of adsorption. The hydrophobic and more hydrophilic nature of ZIF-71 and ZIF-90, respectively, is clearly visible from the obtained values: 16 $kJ \cdot mol^{-1}$ and 36 $kJ \cdot mol^{-1}$, approximately. They are much and just slightly lower than the heat of vaporization of water, which is 40.9 $kJ \cdot mol^{-1}$ using the same water model,[37] in consistency with the experimental value (about 44 $kJ \cdot mol^{-1}$ at 25 ºC).[44,45] It is thus energetically unfavorable for water to break hydrogen bonds in the bulk phase and then be adsorbed in ZIF-71, which explains the forced water intrusion by applying pressure. With increasing loading, the adsorption energy monotonically decreases to about 5 $kJ \cdot mol^{-1}$ in ZIF-71 and to 15 $kJ \cdot mol^{-1}$ in ZIF-90. Figure 5 **c**ollects the guest-guest and host-guest contributions to the average intermolecular energy as a function of fugacity. The information on the latter has been dealt in Figure 4. Water-water potential energy rapidly decreases after water intrusion down to value of about -35 $kJ \cdot mol^{-1}$ in both ZIFs. More specifically, the energy is slightly lower in ZIF-71, which is consistent with its hydrophobic character. The obtained values are somewhat lower (in absolute value) than potential energy for the bulk state, reported above, indicating a dense adsorbed phase with weaker water–water interactions.

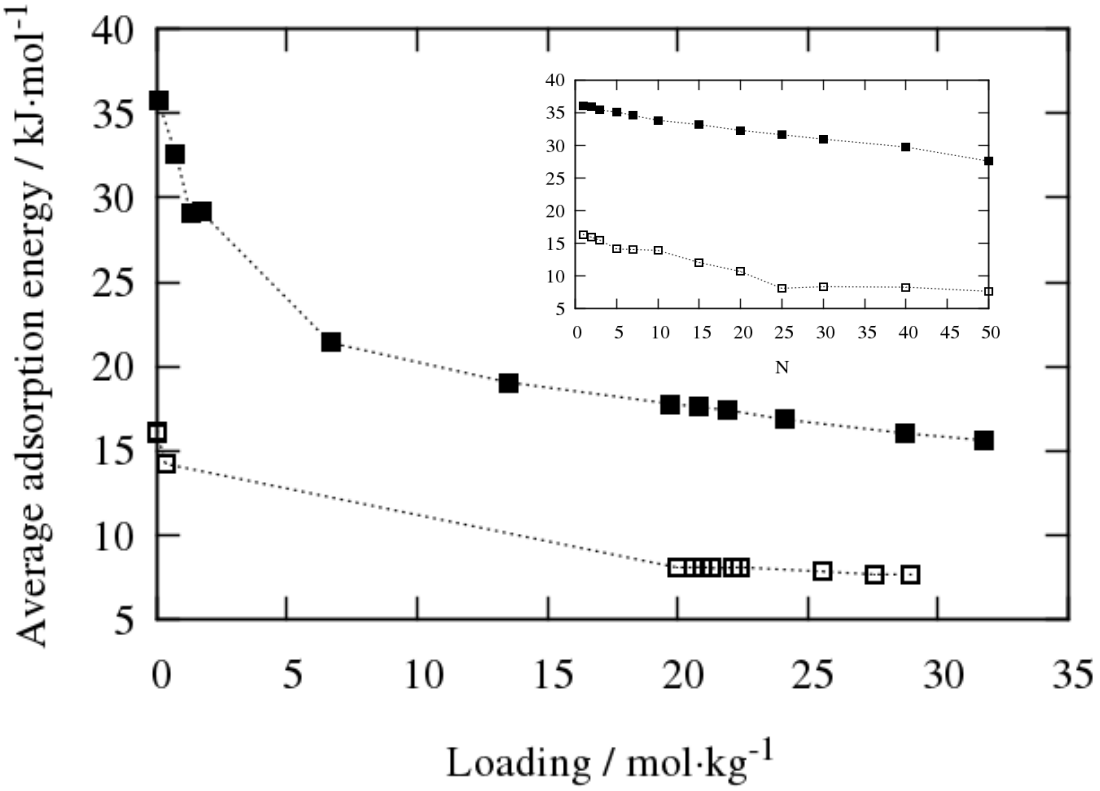

Figure 4. Average adsorption energy ($U_{host-guest} - RT$) as a function of the loading for water in ZIF-71 (empty squares) and in ZIF-90 (full squares). Results of the inset figure were obtained from NVT calculations.

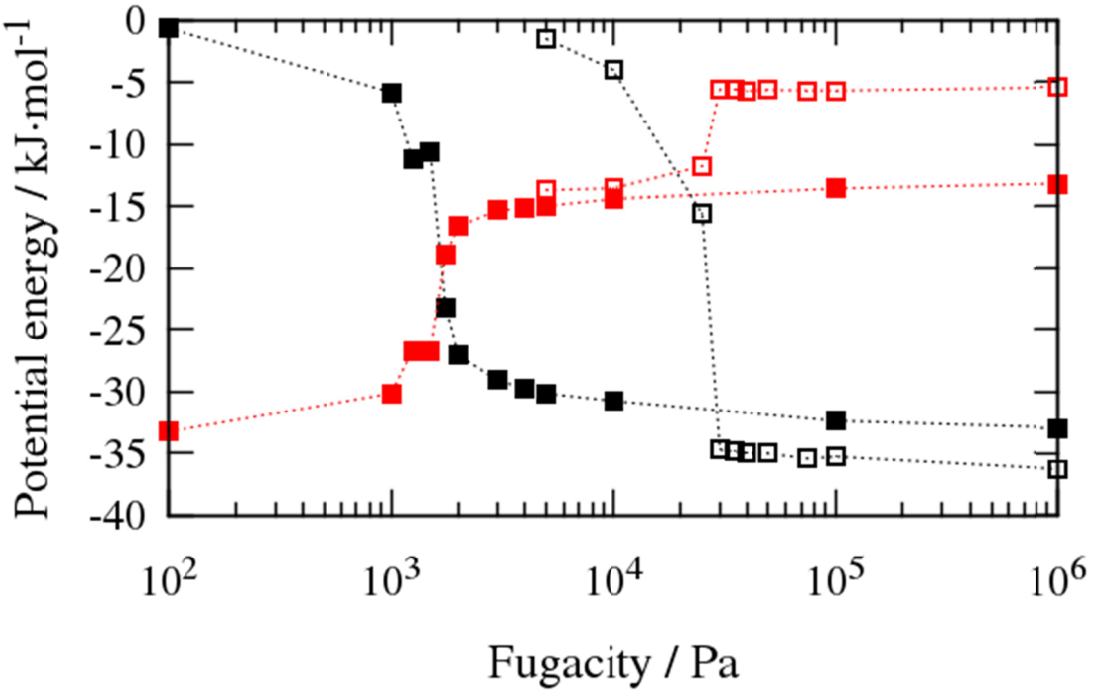

Figure 5. Guest-guest (black) and host-guest (red) contributions to the intermolecular average potential energy in ZIF-71 (empty squares) and ZIF-90 (full squares) as a function of fugacity.

The energetic analysis gives information on the interaction of the adsorbed water molecules with the structure and on self-association governing the adsorption mechanisms. The radial distribution functions $g(r)$ likewise aid to understand the microscopic behavior of the water molecules inside the pores by providing information on the average intermolecular distance and the presence of hydrogen bonds. Figure 6 displays the RDFs in both ZIFs for similar water loadings of about 20 $mol \cdot kg^{-1}$ (after condensation transition). Calculations correspond to water oxygen atoms with each other, and with the framework atoms in order to identify preferential adsorption sites. As reveals the positions of the first peaks in Figure 6a, water-water interactions are notably greater than water-host interactions

in ZIF-71, denoting the hydrophobicity of this ZIF. The g(r) of water around Zn framework atoms of the ZIF reveals negligible interaction. The strongest affinity with water corresponds to chlorine atoms of the functional group, with evident first peaks at distances below 4 Å. In the second stage, the hydrophilicity of ZIF-90 (Fig. 6b) arises from interactions of water molecules with the aldehyde oxygen atoms. The strength of this interaction is comparable with water-water interactions. Indeed, both first peaks, of $O_w - O_{ald}$ and $O_w - O_w$ RDFs, are located at almost the same position: 2.75 Å. This suggests hydrogen bonding formation between water molecules and ZIF-90. Particularly, as apparent from the O-H RDFs depicted in Figure S2 of the ESI, water is the H-bond donor. Interactions of water molecules with the remaining framework atoms are relatively insignificant. As reveals Figure S3 of the ESI, these results characterising interactions of water molecules with the surface of ZIF-90 are kept regardless of fugacity, and so of water loading. Note however that at the highest pressure (Figure S3 d), a clear broadening of the peak in $O_w - O_{ald}$ RDF is observed, denoting a weakening of this cross hydrogen bonding. This is likely due to the strong water-water interactions in the highly hydrated structure.

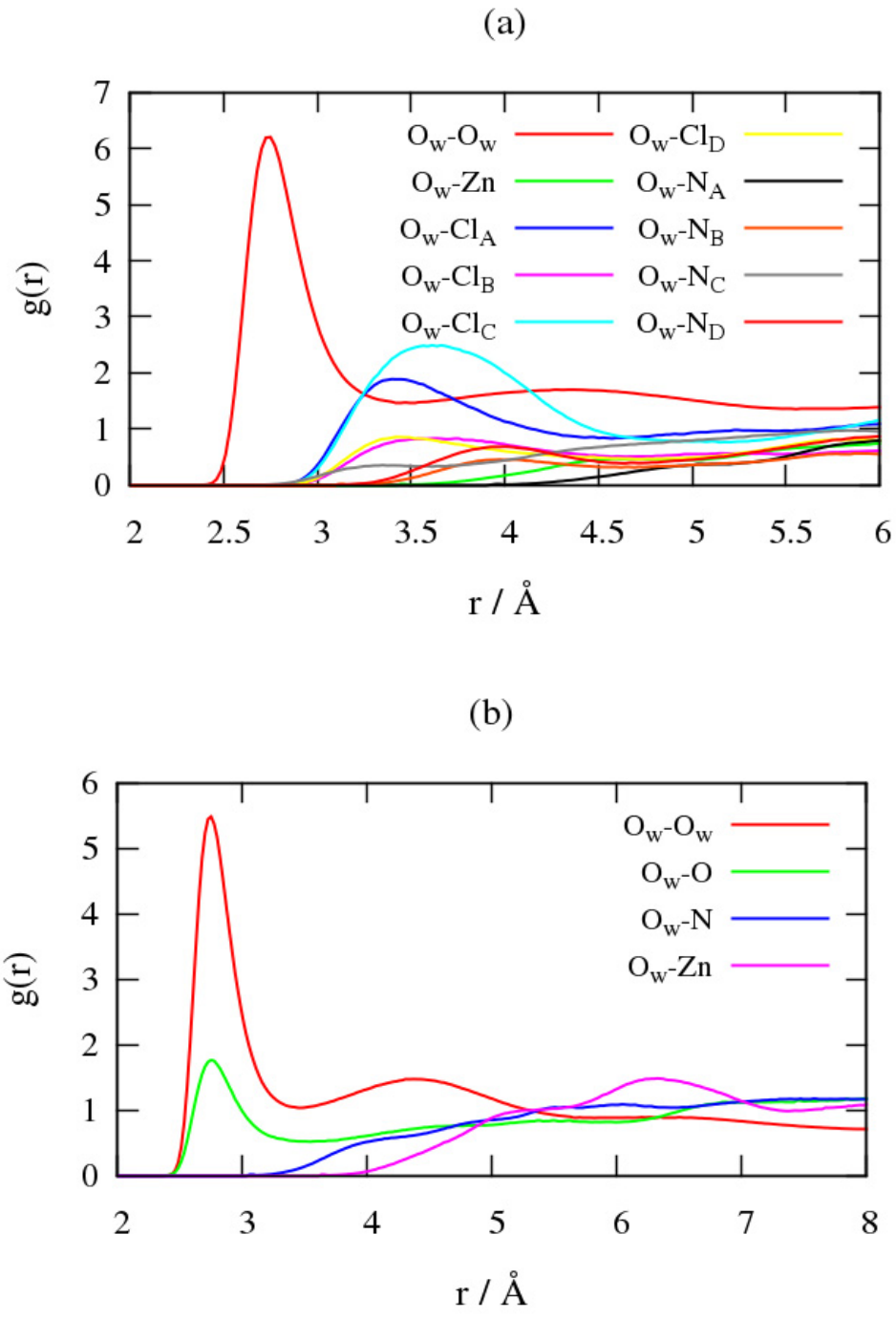

Figure 6. Radial Distribution Functions of the oxygen atoms of adsorbed water molecules O_w between each other and with the framework atoms in ZIF-71 (a) and ZIF-90 (b) for similar water loadings of about 20 mol·kg^{-1} (at 40 kPa and 4 kPa, respectively).

To gain insights into the interactions of water with the structure, we compute the average minimum distances of water (oxygen atom) to the strongest interacting framework sites (chlorine in ZIF-71 and aldehyde oxygen in ZIF-90) in the dilute regime using the NVT ensemble. Results are collected in Figure 7. For a single molecule in the system, this magnitude is 3.7 Å and 3 Å approximately in ZIF-70 and ZIF-90, respectively. These average minimum distances decrease with the number of water molecules *N* until values slightly above 3 Å for ZIF-71 and 2.5 Å for ZIF-90, supporting the weakly polar and rather polar nature of –Cl and –CHO functional groups, respectively. The larger values corresponding to the location of the involved first peaks in the above RDFs evidences weaker interaction of water with the pore surface after condensation in consistency with energetic analysis.

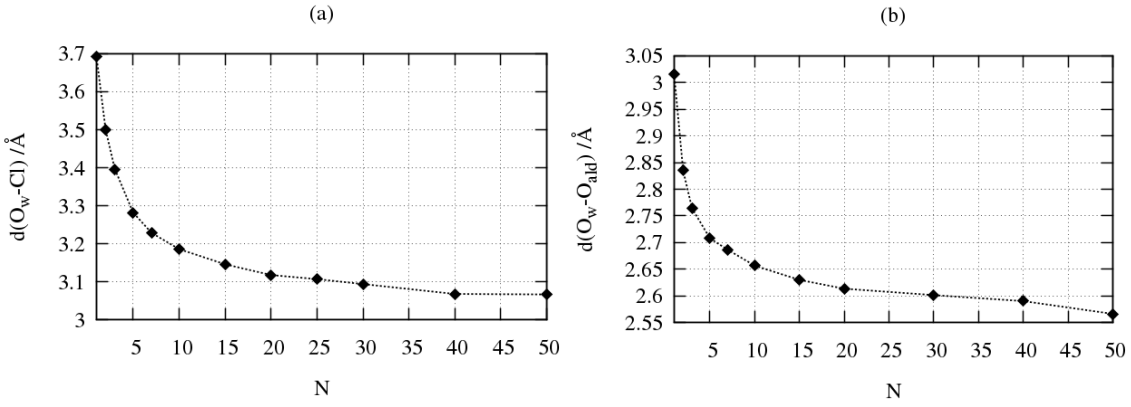

Figure 7. Average minimum distances from oxygen atom of water $\boldsymbol{O_w}$ to $\boldsymbol{Cl}$ in ZIF-71 (a), and to $\boldsymbol{O_{ald}}$ in ZIF-90 (b) as a function of the number of adsorbed water molecules *N* from NVT calculations.

In the following lines, we focused on water-water interactions. The O-O and O-H RDFs of the adsorbed water in the ZIFs at saturation are given in Figure S4 of the ESI together with those for bulk water. We find a strong ordering of water molecules at short distance in both materials, with a remarkable O–O first peak at 2.8 Å as for bulk water. Nevertheless, there is no longer-range order since the second solvation shell characterizing bulk water is absent. This is due to excluded volume effects. The O–H RDF for the adsorbed water in the highly hydrated structures and bulk water is virtually the same: Two distinct peaks at 1.9 Å and 3.2 Å characteristic of hydrogen bonding. This correspondence between the RDFs lead one to conclude that the structure of water adsorbed in the ZIF pores at saturation is similar to bulk liquid water.[32] This result is reasonable taken the large pore sizes of the ZIFs into account. The large available space allows a large number of neighboring water molecules promoting hydrogen bonding. However, here we further investigated the water hydrogen-bonded network through HB statistics, which have been evaluated using a geometric criterion of HB definition.[42] We found appreciable differences of adsorbed water not only with respect to the bulk but also induced by the nature of the ZIF. Particularly, Table 2 shows the obtained values of the fraction of associated (linked through hydrogen bonds) molecules $\boldsymbol{f_{ass}}$, of the percentage of the latter engaged in *i*=1-5 hydrogen bonds $\boldsymbol{f_i}$, and of the average number of hydrogen bonds per molecule $\boldsymbol{n_{HB}}$ for bulk water[43] and adsorbed water at the highest considered pressure. While $\boldsymbol{f_{ass}}$ is virtually 1 for all the systems, differences in the HB populations are clearly apparent. The tetrahedral ordering of bulk water is reflected on the high percentages of $\boldsymbol{f_3}$ and $\boldsymbol{f_4}$, which are virtually the same and about 38 % using the same water model.[37] This results in a $\boldsymbol{n_{HB}}$ value of 3.2. Although adsorbed water retains bulk liquid-like characteristics ($\boldsymbol{f_3} \sim$ 40 %), the

percentage of water molecules engaged in 4 hydrogen bonds considerably decreases in favor to mainly f_2. The main difference between water adsorbed in ZIF-71 and ZIF-90 lie in this variation: While f_2 and f_4 are almost the same and about 25 % in ZIF-71, f_2 largely overcomes f_4 in the case of ZIF-90. These results lead to the respective n_{HB} values of 2.9 and 2.7. Thus, despite the larger porosity of ZIF-90, we found a slightly more complex water HB network in ZIF-71. This is consistent with guest-guest interactions reported for both ZIFs in Figure 5. Although framework topology can greatly affect,[43] here this is likely due to the virtual lack of interactions with the pore surface in ZIF-71.

Table 2. HB statistics of bulk water and of water adsorbed in ZIF-71 and ZIF-90 at 10^6 Pa.

	f_{ass}	f_1	f_2	f_3	f_4	f_5	n_{HB}
Bulk[43]	0.99	3.9	17.4	38.3	38.0	2.4	3.2
ZIF-71	0.97	7.1	23.6	40.9	25.6	2.7	2.9
ZIF-90	0.98	7.8	30.9	43.6	16.4	1.25	2.7

Figures 8 and 9 show the results of the previous magnitudes as a function of fugacity in order to examine H-bonding during the adsorption process. Figure 8a shows a steep increase up to roughly 1 of the fraction of associated molecules f_{ass} in both ZIFs at about their respective onset pressures of adsorption. As can be seen in Figure 8b, the behavior of n_{HB} as a function of fugacity is in close relation with the adsorption performance in both ZIFs. The hydration mechanism proceeding through water cluster formation and growth in hydrophobic materials such as ZIF-71 was expected.[43,46] However, this result reveals that the rapid pore filling is also owing to water clustering even in ZIF-

90, rather than to nucleation around the high-energy sites (the aldehyde oxygen framework atoms). We can thus conclude for the latter that the polar formyl groups in Im linkers shifts the onset adsorption pressure to below the bulk saturation pressure, but the mechanisms of pore filling keep being governed by molecular association of water. This finding supports an amphiphilic character for this ZIF. In Figure 9, we plot the HB populations as a function of fugacity. Stable values, previously discussed in Table 2, are reached from the lowest pressures of adsorption, especially in the purely hydrophobic ZIF-71. This corroborates the rapid formation of the dense phase by self-association.

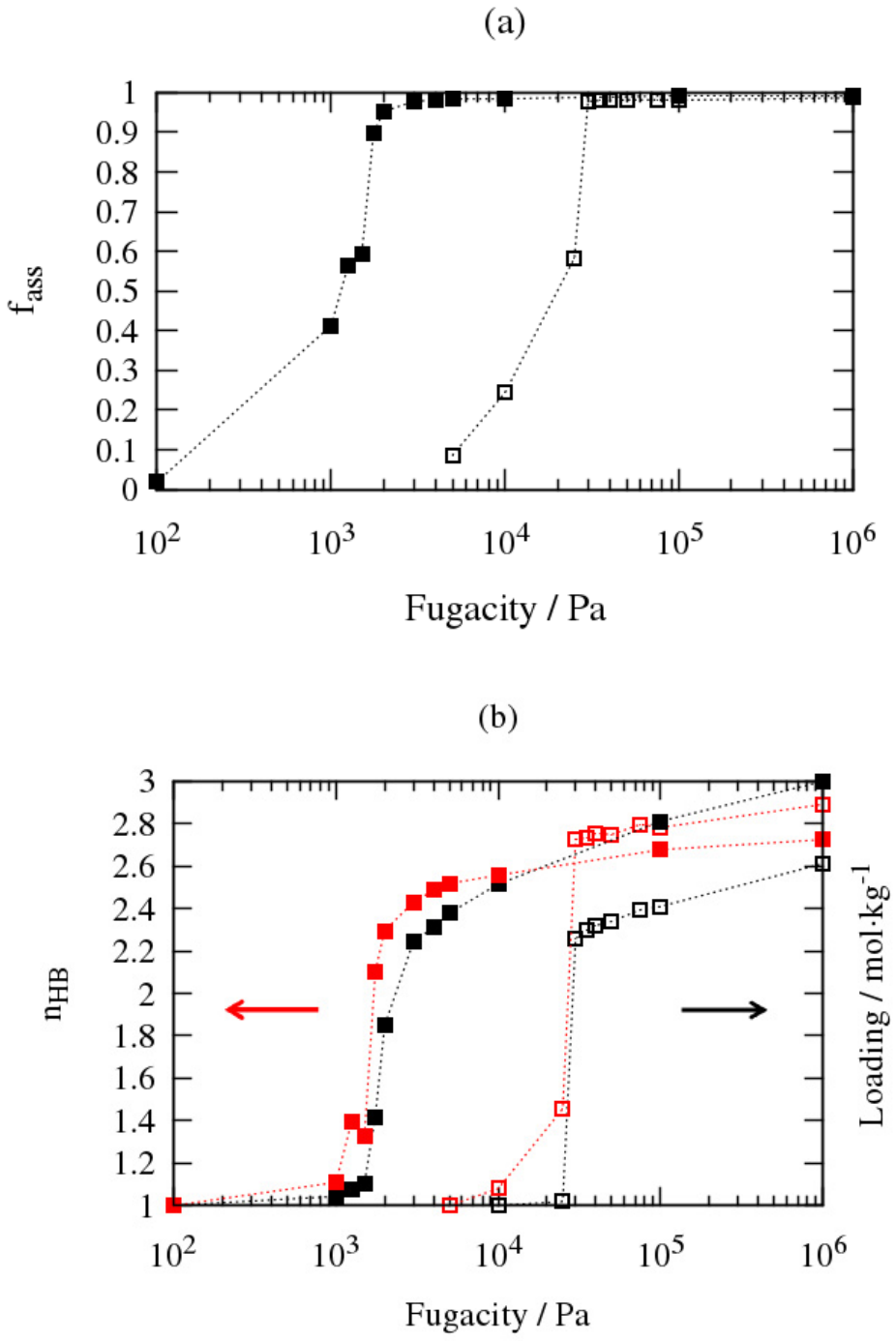

Figure 8. Fraction of associated water molecules f_{ass} (a), and average number of hydrogen bonds per molecule n_{HB} (red) together with the loading (black) (b) as a function of fugacity in ZIF-71 (empty squares) and ZIF-90 (full squares).

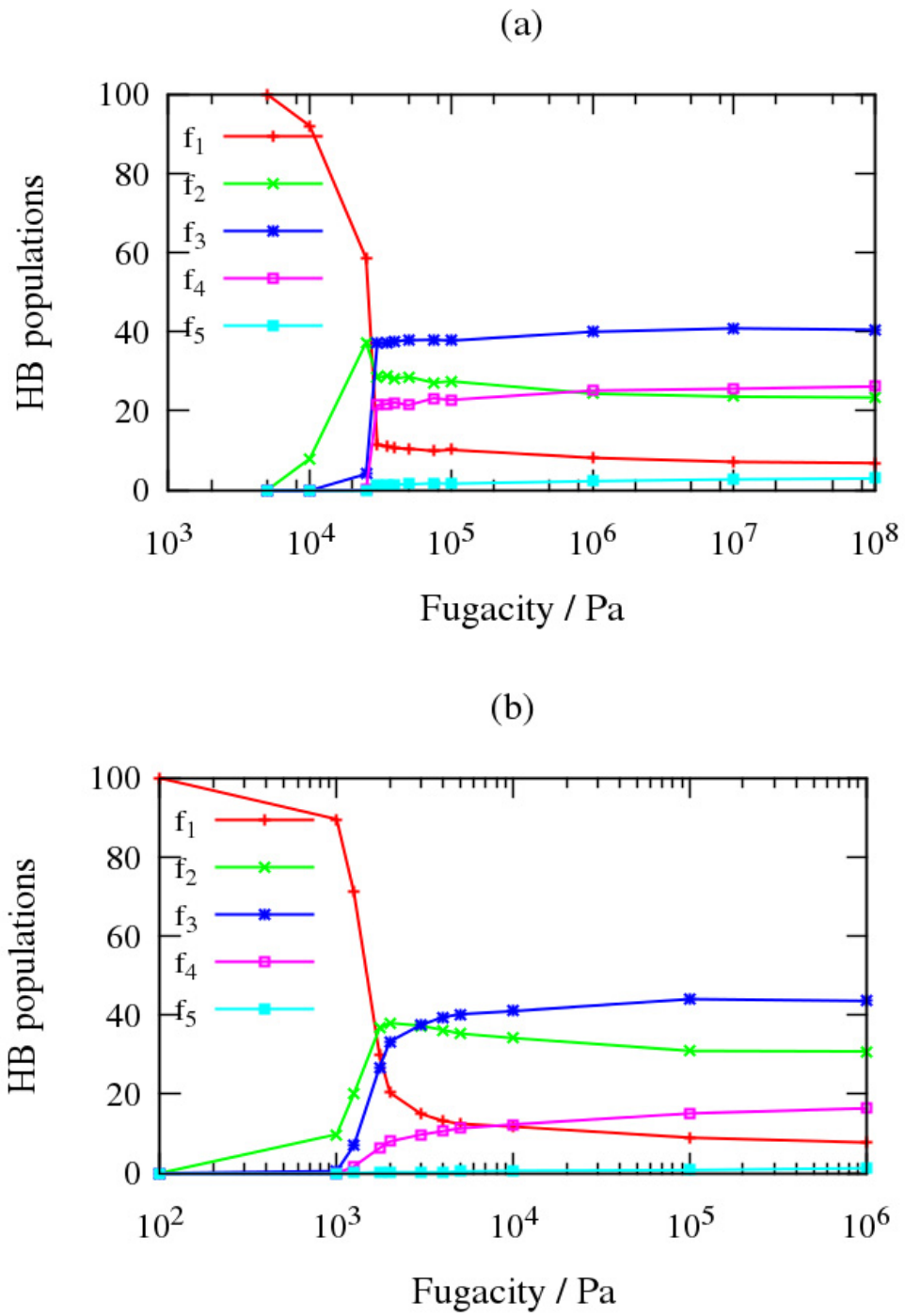

Figure 9. Percentage of water molecules engaged through 1-5 hydrogen bonds ($f_1 - f_5$) as a function of fugacity in ZIF-71 (a) and ZIF-90 (b).

4. Conclusions

By using molecular simulation, we characterized the microscopic behavior governing the adsorption performance of water in two substantially different ZIFs concerning topology and composition, and so nature, namely ZIF-71 and ZIF-90. We computed the adsorption isotherms of water in both ZIFs at 298 K via Monte Carlo simulations in the grand canonical ensemble. Although chlorine functional group of ZIF-71 is weakly polar as reflects the adsorption in the liquid phase (hydrophobic nature), its interaction with water molecules is remarkable in relation to the remaining framework atoms, as reveals the Radial Distribution Functions. In ZIF-90, the aldehyde oxygen atom was distinctly found the strongest interacting site surely involving hydrogen bonds with water molecules, and thus responsible of the water intrusion below the bulk saturation pressure (hydrophilic nature). The affinity of water to these preferential sites in each ZIF, *Cl* and O_{ald}, was quantitatively evaluated in terms of the adsorption energy and the average minimum distances in the low-coverage regime from NVT calculations. The distance values for a single water molecule in the system were found 3.7 Å in ZIF-71 and 3 Å in ZIF-90, with respective heats of adsorption of 16 $kJ \cdot mol^{-1}$ and 36 $kJ \cdot mol^{-1}$, approximately. The abrupt condensation transition observed in the water adsorption isotherms in both ZIFs was demonstrated, by means of energetic and structural factors, consequence of rapid water clustering even in ZIF-90. Instead of nucleation around the O_{ald} high-energy sites, self-association of water dominates the adsorption process, as in hydrophobic materials such as ZIF-71. This suggests an amphiphilic more than hydrophilic character of ZIF-90. Indeed, the adsorption energy in dilute regime was found even slightly lower than the heat of vaporization of water, and significantly decreases with water uptake. In the highly hydrated structures, the HB properties of water reveal the absence of the tetrahedral ordering typical

of the bulk in both ZIFs, and the formation of higher-order water clusters in ZIF-71 despite its lower accessible space in comparison with ZIF-90. This is ascribed to the weaker interactions with the pore surface, which enhances hydrogen bonding formation between water molecules.

Supporting Information: Pore Size Distributions of ZIF-71 and ZIF-90, and complementary Radial Distribution Functions characterizing the structure of the adsorbed water molecules and interactions with the framework atoms. This material is available free of charge via the Internet at http:// pubs.acs.org/.

Acknowledgements

This work is supported by the European Research Council through an ERC Starting Grant (ERC2011-StG-279520-RASPA), by the MINECO (CTQ2013-48396-P) and by the Andalucía Region (FQM-1851).

References

(1) Yaghi, O. M.; O'Keefe, M.; Ockwig, N. W.; Chae, H. K.; Eddaoudi, M.; Kim, J. Reticular Synthesis and the Design of New Materials. *Nature* **2003**, *423*, 705-714.

(2) Férey, G. Hybrid Porous Solids: Past, Present, Future. *Chem. Soc. Rev.* **2008**, *37*, 191–214.

(3) Zhou, H. C.; Long, J. R.; Yaghi, O. M. Introduction to Metal–Organic Frameworks. *Chem. Rev.* **2012**, *112*, 673–674.

(4) *Metal–Organic Frameworks: Applications from Catalysis to Gas Storage*, ed. D. Farrusseng, Wiley-VCH, Weinheim, 2011.

(5) Horike, S.; Shimomura, S.; Kitagawa, S. Soft Porous Crystals. *Nat. Chem*. **2009**, *1*, 695–704.

(6) Farha, O. K.; Hupp, J. T. Rational Design, Synthesis, Purification, and Activation of Metal-Organic Frameworks Materials. *Acc. Chem. Res*. **2010**, *43*, 1166–1175.

(7) Tranchemontagne, D. J.; Mendoza-Cortes, J. L.; O'Keeffe, M.; Yaghi, O. M. Secondary Building Units, Nets and Bonding in the Chemistry of Metal-Organic Frameworks. *Chem. Soc. Rev*. **2009**, *38*, 1257–1283.

(8) Li, J.-R.; Kuppler, R.-J.; Zhou, H.-C. Selective Gas Adsorption and Separation in Metal–Organic Frameworks. *Chem. Soc. Rev.* **2009**, *38*, 1477-1504.

(9) Ma, S.; Zhou, H. C. Gas Storage in Porous Metal–Organic Frameworks for Clean Energy Applications. *Chem. Commun.* **2010**, *46*, 44-53.

(10) Wu, H.; Zhou, W.; Yildirim, T. Methane Sorption in Nanoporous Metal−Organic Frameworks and First-Order Phase Transition of Confined Methane. *J. Phys. Chem. C* **2009**, *113*, 3029–3035.

(11) Zhang, Z.; Zhao, Y.; Gong, Q.; Li, Z.; Li, J. MOFs for CO_2 Capture and Separation from Flue Gas Mixtures: The Effect of Multifunctional Sites on their Adsorption Capacity and Selectivity. *Chem. Commun*. **2013**, *49*, 653-66.

(12) Burtch, N. C.; Jasuja, H.; Walton, K. S. Water Stability and Adsorption in Metal−Organic Frameworks, *Chem. Rev.* **2014**, *114*, 10575−10612.

(13) Paranthaman, S.; Coudert, F.-X.; Fuchs, A. H. Water Adsorption in Hydrophobic MOF Channels, *Phys. Chem. Chem. Phys*. **2010**, *12*, 8123–8129.

(14) Ghosh, P.; Kim, K. C.; Snurr, R. Q. Modeling Water and Ammonia Adsorption in Hydrophobic Metal−Organic Frameworks: Single Components and Mixtures *J. Phys. Chem. C* **2014**, *118*, 1102−1110.

(15) Liu, Y. L.; Kravtsov, V. C.; Larsen, R.; Eddaoudi, M. Molecular Building Blocks Approach to the Assembly of Zeolite-like Metal-Organic Frameworks with Extra-large Cavities. *Chem.Commun.* **2006**, *42*, 1488-1490.

(16) Park, K. S.; Ni, Z.; Cote, A. P.; Choi, J. Y.; Huang, R. D.; Uribe-Romo, F. J.; Chae, H. K.; O'Keeffe, M.; Yaghi, O. M. Exceptional Chemical and Thermal Stability of Zeolitic Imidazolate Frameworks. *Proc. Natl. Acad. Sci. U.S.A.* **2006**, *103*, 10186-10191.

(17) Phan, A.; Doonan, C. J.; Uribe-Romo, F. J.; Knobler, C. B.; O'Keeffe, M.; Yaghi, O. M. Synthesis, Structure, and Carbon Dioxide Capture Properties of Zeolitic Imidazolate Frameworks. *Acc. Chem. Res.* **2010**, *43*, 58-67.

(18) Banerjee, R.; Phan, A.; Wang, B.; Knobler, C.; Furukawa, H.; O'Keeffe, M.; Yaghi, O. M. High-Throughput Synthesis of Zeolitic Imidazolate Frameworks and Application to CO_2 Capture. *Science* **2008**, *319*, 939–943.

(19) Wang, B.; Cote, A. P.; Furukawa, H.; O'Keeffe, M.; Yaghi, O. M. Colossal Cages in Zeolitic Imidazolate Frameworks as Selective Carbon Dioxide Reservoirs. *Nature* **2008**, *453*, 207-211.

(20) Liu, D.-H.; Zheng, C.-C.; Yang, Q.-Y.; Zhong, C.-L. Understanding the Adsorption and Diffusion of Carbon Dioxide in Zeolitic Imidazolte Frameworks: A Molecular Simulation Study. *J. Phys. Chem. C* **2009**, *113*, 5004-5009.

(21) Rankin, R. B.; Lin, J. C.; Kulkarni, A. D.; Johnson, J. K. Adsorption and Diffusion of Light Gases in ZIF-68 and ZIF-70: A Simulation Study. *J. Phys. Chem. C* **2009**, *113*, 16906-16914.

(22) Liu, Y.; Liu, H. L.; Hu, Y.; Jiang, J. W. Development of a Density Functional Theory in Three-Dimensional Nanoconfined Space: H_2 Storage in Metal-Organic Frameworks. *J. Phys. Chem. B* **2009**,*113*, 12326-12331.

(23) Li, K. H.; Olson, D. H.; Seidel, J.; Emge, T. J.; Gong, H. W.; Zeng, H. P.; Li, J. Zeolitic Imidazolate Frameworks for Kinetic Separation of Propane and Propene. *J. Am. Chem. Soc.* **2009**, *131*, 10368-10369.

(24) Perez-Pellitero, J.; Amrouche, H.; Siperstein, F. R.; Pirngruber, G.; Nieto-Draghi, C.; Chaplais, G.; Simon-Masseron, A.; Bazer-Bachi, D.; Peralta, D.; Bats, N. Adsorption of CO_2, CH_4, and N_2 on Zeolitic Imidazolate Frameworks: Experiments and Simulations. *Chem. – Eur. J.*, **2010**, *16*, 1560-1571.

(25) Küsgens, P.; Rose, M.; Senkovska, I.; Fröde, H.; Henschel, A.; Siegle, S.; Kaskel, S. Characterization of Metal-Organic Frameworks by Water Adsorption. *Microporous Mesoporous Mater*. **2009**, *120*, 325–330.

(26) Ortiz, G.; Nouali, H.; Marichal, C.; Chaplais, G.; Patarin, J. Energetic Performances of the Metal-Organic Framework ZIF-8 Obtained Using High Pressure Water Intrusion-Extrusion Experiments. *Phys. Chem. Chem. Phys*. **2013**, *15*, 4888–4891.

(27) Zhang, K.; Lively, R. P.; Zhang, C.; Koros W. J.; Chance, R. R. Investigating the Intrinsic Ethanol/Water Separation Capability of ZIF-8: An Adsorption and Diffusion Study. *J. Phys. Chem. C* **2013**, *117*, 7214–7225.

(28) Lively, R. P.; Dose, M. E.; Thompson, J. A.; McCool, B. A.; Chance, R. R.; Koros, W. J. Ethanol and Water Adsorption in Methanol-Derived ZIF-71. *Chem. Commun*., **2011**, *47*, 8667–8669.

(29) Nalaparaju, A.; Zhao, X. S.; Jiang, J. W. Molecular Understanding for the Adsorption of Water and Alcohols in Hydrophilic and Hydrophobic Zeolitic Metal-Organic Frameworks. *J. Phys. Chem. C* **2010**, *114*, 11542–11550.

(30) Amrouche, H.; Creton, B.; Siperstein, F.; Nieto-Draghi, C. Prediction of Thermodynamic Properties of Adsorbed Gases in Zeolitic Imidazolate Frameworks. *RSC Adv*. **2012**, *2*, 6028–6035.

(31) Zhang, K.; Lively, R. P.; Dose, M. E.; Brown, A. J.; Zhang, C.; Chung, J.; Nair, S.; Koros, W. J.; Chance, R. R. Alcohol and Water Adsorption in Zeolitic Imidazolate Frameworks. *Chem. Commun*. **2013**, *49*, 3245–3247.

(32) Ortiz, U.; Freitas, A. P.; Boutin, A.; Fuchs, A. H.; Coudert, F-X. What Makes Zeolitic Imidazolate Frameworks Hydrophobic or Hydrophilic? The Impact of Geometry and Functionalization on Water Adsorption. *Phys. Chem. Chem. Phys.* **2014**, *16*, 9940-9949.

(33) Zhang, K.; Nalaparaju, A.; Chen, Y.; Jiang, J. Biofuel Purification in Zeolitic Imidazolate Frameworks: the Significant Role of Functional Groups. *Phys. Chem. Chem. Phys.* **2014**, *16*, 9643-9655.

(34) Frenkel, D.; Smit, B. *Understanding Molecular Simulation*; Academic Press: San Diego, CA, 1996.

(35) Morris, W.; Doonan, C. J.; Furukawa, H.; Banerjee, R; Yaghi, O. M. Crystals as Molecules: Postsynthesis Covalent Functionalization of Zeolitic Imidazolate Frameworks. *J. Am. Chem. Soc*. **2008**, *130*, 12626-12627.

(36) Willems, T. F.; Rycroft, C. H.; Kazi, M.; Meza, J. C.; Haranczyk, M. Algorithms and Tools for High-Throughput Geometry-Based Analysis of Crystalline Porous Materials. *Microporous Mesoporous Mater*. **2012**, *149*, 134-141.

(37) Rick, S. A Reoptimization of the Five-Site Water Potential (Tip5p) for Use with Ewald Sums. *J. Chem. Phys.* **2004**, *120*, 6085-6093.

(38) Mayo, S. L.; Olafson, B. D.; Goddard, W. A. DREIDING: a Generic Force Field for Molecular Simulations. *J. Phys. Chem*. **1990**, *94*, 8897-8909.

(39) Dubbeldam, D.; Torres-Knoop, A.; Walton, K. S. On the Inner Workings of Monte Carlo Codes. *Mol. Simul.* **2013**, *39*, 1253-1292.

(40) Dubbeldam, D.; Calero, S.; Donald, E.; Snurr, R. RASPA: Molecular Simulation Software for Adsorption and Diffusion in Flexible Nanoporous Materials. *Mol. Simul.* **2015**, DOI 10.1080/08927022.2015.1010082.

(41) Robinson, D. B.; Peng, D. Y.; Chung, S. Y. K. The Development of the Peng-Robinson Equation and its Application to Phase-Equilibrium in a System Containing Methanol. *Fluid Phase Equilib.* **1985**, *24*, 25-41.

(42) Luzar, A.; Chandler, A. Structure and Hydrogen Bond Dynamics of Water-Dimethyl Sulfoxide Mixtures by Computer Simulations. *J. Chem. Phys*. **1993**, *98*, 8160–8173.

(43) Calero, S.; Gómez-Álvarez, P. Hydrogen Bonding of Water Confined in Zeolites and their Zeolitic Imidazolate Framework counterparts. *RSC Adv.* **2014**, *4*, 29571–29580.

(44) Lange, N. A. *Handbook of Chemistry*, McGraw-Hill, New York, 1956.

(45) Marsh, K. N. *Recommended Reference Materials for the Realization of Physicochemical Properties*, Blackwell, Oxford, 1987.

(46) Desbiens, N.; Demachy, I.; Fuchs, A. H.; Kirsch-Rodeschini, H.; Soulard, M.; Patarin, J. Water Condensation in Hydrophobic Nanopores. *Angew. Chem., Int. Ed*. **2005**, *44*, 5310−5313.

Table of Contents Image